JOURNAL OF Materials CHEMISTRY

Structures of nanosized Fe–Ti mixed oxide particles produced by freezing method

Tatsuo Ishikawa,*[a] Tomoya Ueno,[a] Akemi Yasukawa,[a] Kazuhiko Kandori,[a] Takenori Nakayama[b] and Takayuki Tsubota[b]

[a]*School of Chemistry, Osaka University of Education, 4-698-1 Asahigaoka, Kashiwara, Osaka 582-8582, Japan. E-mail: ishikawa@cc.osaka-kyoiku.ac.jp; Fax: +81-729-78-3394*
[b]*Materials Research Laboratory, Kobe Steel Ltd., 5-5 Takatsukadai, 1-chome, Nishi-ku, Kobe, Hyogo 615-2271, Japan*

Received 11th March 2002, Accepted 1st May 2002
First published as an Advance Article on the web 12th June 2002

Fe–Ti mixed oxide nanoparticles with different atomic ratios in Ti/(Fe + Ti) from 0 to 1.0 have been prepared by hydrolysis of aqueous solutions containing Fe(III) and Ti(IV) ions and a freezing method with liquid N_2, which inhibits crystallization and particle growth. The particles produced were poorly crystalline according to XRD and the product, in the absence of Ti(IV), was assigned to 2-line ferrihydrite. The products had a high specific surface area of 369–460 $m^2\ g^{-1}$, corresponding to a mean particle size of 3–4 nm. These nanosized particles were composed of crystallites of about 1 nm size. It was found by Mössbauer spectroscopy that the particles produced were superparamagnetic and their blocking temperature and inner electric field decreased with increasing Ti(IV) content.

Introduction

Nanostructured metal oxide particles engender much attention with regard to their electrical, magnetic, optical and catalytic characteristics, which are anticipated to be different from the properties of the bulk particles.[1–4] Although many preparation methods of metal oxide particles have been developed, particle preparation from aqueous metal salt solutions surpasses other methods in terms of controlling the particle composition and morphology, high yield production, synthesis under a mild conditions with low energy consumption, and applicability for various substances. Among the various preparation methods from aqueous solution, the most popular and facile technique is hydrolysis of metal ions. However, the hydrolysis method is frequently not available for preparation of nanoparticles, because the particle growth is too rapid to produce fine particles. To suppress the particle growth, various methods have been employed; for instance, addition of chelating agents and matrices such as microemulsions, polymers and inorganic gels. The main disadvantage of these methods is the difficulty in producing particles free from impurities. A noteworthy and rather easy method to inhibit particle growth has been developed by van der Giessen.[5,6] Iron oxide nanoparticles were prepared with a *ca.* 3 nm diameter by hydrolysis employing a freezing method to inhibit particle growth; freezing with liquid nitrogen isolated the powders (consisting of the nanoparticles) from the gels formed by hydrolyzing an $Fe(NO_3)_3$ solution. The freezing method impedes the crystallization of the ferric hydroxide gels formed and also the particle growth by dehydration, so producing fine particles. Another merit of this method is the easy separation of the particles formed from the gels which saves separation and washing time, resulting in prevention of particle growth.

Nanoparticles of Fe(III)–Ti(IV) mixed oxides are attractive for application as photocatalysts, which may be sensitive to visible light. Moreover, Fe(III) oxide nanoparticles are a major component of steel rusts. Recently, the influence of anti-corroding alloying metals such Ti, Cu, Ni and Cr on the structure of amorphous rust has become an important subject in corrosion science, because the poorly crystalline rusts are thought to form dense layers resistant to corrosion. We have investigated the effect of Ti(IV) on the formation and structure of various rust components such as α-, β- and γ-FeOOH[7–9] and Fe_3O_4.[9] Nevertheless, the detailed structures, especially short range structures, of the poorly crystallized Fe–Ti mixed oxides have not been thoroughly investigated. For this reason, in the present study, nanoparticles of Fe–Ti mixed oxides were prepared by the freezing method. The resultant particles were characterized by Mössbauer spectroscopy which provides information on the local structures of the less crystallized materials. The results presented in this paper may serve to develop novel photocatalysts and also to understand the role of Ti in the anti-corroding of steels.

Experimental details

Materials

50 cm^3 solutions containing 0.05 mol $Fe(NO_3)_3$ and $Ti(SO_4)_2$ at different atomic ratios of 0–1.0 in Ti/(Fe+Ti) were prepared. To the solutions cooled at 0 °C a 14.5 mol dm^{-3} NH_4OH solution was rapidly added with stirring, by which the solution pH was adjusted to more than 9. Liquid nitrogen was instantaneously poured into the resultant gels in a porcelain dish to freeze the gels. After defrosting at room temperature, the precipitates were filtered off and washed with water until no NH_4^+ was detected in the filtrate by Nessler's reagent, and finally dried *in vacuo* at room temperature.

Characterization

The materials produced as described above were characterized by the following complementary means. Powder X-ray diffraction (XRD) was carried out by a Rigaku diffractometer using a CuKα irradiation at 200 mA and 40 kV. IR spectra of the products were recorded with a Nicolet FTIR spectrometer by a KBr method. Morphology of the particles was observed by a JEOL transmission electron microscope (TEM). Fe and Ti in the products were assayed using a Seiko induction coupled plasma (ICP) spectrometer by dissolving the samples in a concentrated HCl solution and diluting to the desired concentration with water. The N content of the particles was

 DOI: 10.1039/b202509b

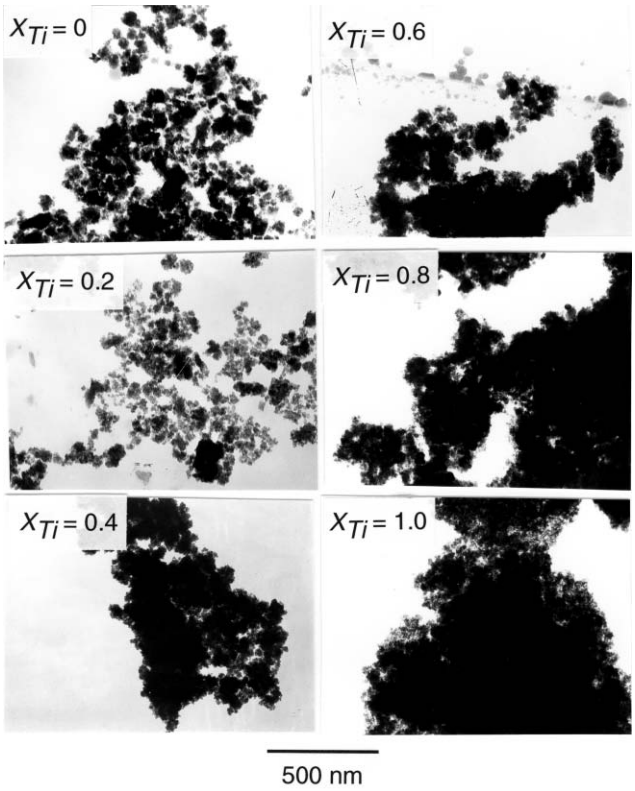

Fig. 1 TEM pictures of the products at various X_{Ti}.

determined by elemental analysis with a Yanagimoto CHN analyzer. Thermogravimetry (TG) and differential thermal analysis (DTA) were simultaneously performed by a Seiko thermoanalyzer at a heating rate of 5 °C min^{-1} in an air stream. Mössbauer spectra were traced at 5–300 K by a Toyo Research spectrometer using a γ-ray source of 1.85 GBq from ^{57}Co diffused in a Rh foil. The transmission spectra obtained were analyzed by least-squares fitting to the Lorentz function. To determine the specific surface area, which reflected the particle size, the adsorption isotherms of N_2 were measured by an automatic volumetric apparatus at the boiling point of liquid N_2. Prior to adsorption the samples were evacuated at 100 °C for 2 h.

Results and discussion

Morphology

Fig. 1 displays the TEM images of the particles formed. Hereafter the Ti/(Fe+Ti) atomic ratios in the solutions before hydrolysis are referred to as X_{Ti}. It was confirmed by ICP that X_{Ti} in the starting solutions was equivalent to the atomic ratio in the particles formed. Thus, most of the Ti(IV) added into the starting solutions remained in the particles obtained. From observing Fig. 1, all the samples are irregular agglomerates of fine particles and the aggregation becomes noticeable as X_{Ti} increases. Since the particle size could not be determined from

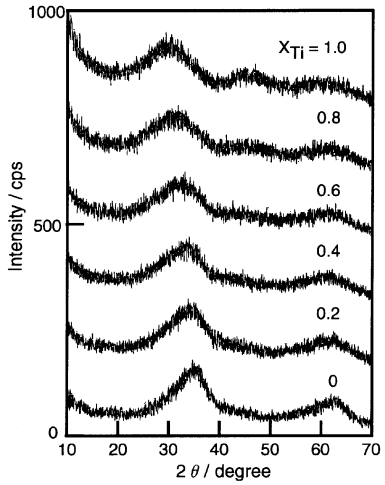

Fig. 2 XRD patterns of the products at various X_{Ti}.

the pictures in Fig. 1, the mean particle sizes were evaluated from the specific surface areas by assuming spherical particles with a density of 3.8 g cm^{-3} as employed by van der Giessen[5] and using the equation, $D_m = 6/(dS)$, where D_m, d and S are mean diameter, density and specific surface area, respectively. The values of D_m obtained are listed in Table 1 and range from 3.3 to 4.1 nm, by which the particles formed are regarded as nanoparticles.

XRD

Fig. 2 depicts the XRD patterns of the products at varied X_{Ti}. Two broad peaks appear on the product at $X_{Ti} = 0$ and three broad peaks are detected on the product at $X_{Ti} = 1.0$. With increasing X_{Ti} the peak at $2\theta = 35°$ (d spacing = 0.26 nm) of the product at $X_{Ti} = 0$ monotonously moves to that at $2\theta = 30°$ ($d = 0.30$ nm) and the weak peak at around $2\theta = 62°$ ($d = 0.15$ nm) slightly shifts to $2\theta = 60°$ ($d = 0.15$ nm) while the weak peak at $2\theta = 45°$ ($d = 0.20$ nm) detected at high X_{Ti} does not move. The peak shift on adding Ti(IV) is attributed to the difference between the ionic radii of Fe(III) [0.064 nm] and Ti(IV) [0.068 nm]. It has been reported that the amorphous precipitates formed on hydrolysis of an $FeCl_3$ solution show only two broad peaks at $d = 0.154$ and 0.252 nm, which have been interpreted as arising from a planar arrangement of tetrameters of edge-shared Fe(O, OH, OH_2) octahedra.[10] The d-values of the two broad peaks detected for the products at $X_{Ti} \leqslant 0.6$ are fairly close to the literature data,[11,12] being indicative of the highly disordered crystal structures of the present materials. It is known that the most distorted ferrihydrite with poor crystallinity and stability gives rise to only two broad bands at about 0.255 and 0.150 nm.[13–15] These d-values are close to those of the material at $X_{Ti} = 0$, allowing us to assign the product as 2-line ferrihydrite. However, the weak peak at $d = 0.20$ nm at high X_{Ti} is not assigned at present. The products at high X_{Ti} are thought to be hydrous Ti(IV) oxide substituted with Fe(III) having a distorted structure of which the detail is unclear at the present. The crystallite sizes of the

Table 1 Composition, specific surface area (S), mean particle size (D_m), crystallite size, mass loss, and N content of the products

X_{Ti} atomic ratio		Surface area (S)/m^2 g^{-1}	Particle size (D_m)/nm	Crystallite size/nm	Mass loss/ mass %	N content/ mass %
Starting solution	Particle					
0		368	4.1	1.1	24	0.05
0.20	0.19	383	3.9	1.0	23	0.12
0.40	0.41	443	3.6	1.0	22	0.41
0.60	0.58	419	3.4	0.9	21	1.00
0.80	0.79	437	3.4	0.8	20	1.60
1.00		460	3.3	0.8	20	2.43

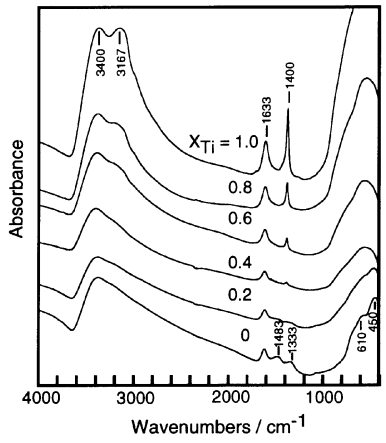

Fig. 3 IR spectra of the products at various X_{Ti}.

products were evaluated from full width at half maximum (FWHM) of the peaks at $d = 0.26$–0.30 nm using the Scherrer equation. The crystallite sizes obtained are shown in Table 1. The average particle size is about 4 times the crystallite size of about 1 nm for each product. It is of interest that the particles are agglomerates of about 4 crystallites, of which the sizes are close to the unit-cell parameters of ferrihydrite ($a = 0.508$ nm and $c = 0.940$ nm).[16]

FTIR

Since the poorly crystalline products were hard to identify from the XRD patterns, IR spectra of the products were taken. They are shown in Fig. 3. The assignment of the bands in the spectra described below was based on the literature.[17] The spectrum of the product at $X_{Ti} = 0$ shows a strong broad stretching vibration band of OH^- and of the OH group of H_2O (3400 cm^{-1}), a weak deformation vibration band of H_2O (1633 cm^{-1}), two weak deformation vibration bands of NO_3^- (1483 and 1333 cm^{-1}) and a strong band at 450 cm^{-1} with a shoulder at around 610 cm^{-1}. The 450 and 610 cm^{-1} bands are assigned to bulk OH deformations of ferrihydrite.[18] From this spectrum the material is identified as ferrihydrite containing NO_3^-. The spectra of the products at $X_{Ti} \geqslant 0.4$ possess bands at 3167 and 1400 cm^{-1} in addition to bands at 3400 and 1633 cm^{-1} while no NO_3^- band appears. The first two bands are assigned to NH_4^+ and are intensified by increasing X_{Ti}. As seen in Table 1, the N content increases with increasing X_{Ti}, as well as the intensity of NH_4^+ band. The precipitates were thoroughly washed with water until no NH_4^+ ions were detected in the eluates, nevertheless the products contain NH_4^+. It seems therefore that NH_4^+ ions are strongly bound in the products though the detailed mechanism remains unexplained. The 1633 and 3400 cm^{-1} bands, due to H_2O molecules, intensify with increasing X_{Ti}, which is caused by the increase of specific surface area (Table 1).

TG-DTA

The FTIR spectra showed the products contained OH^- and H_2O. The content of OH^- and H_2O in the products were estimated by TG. All the TG curves of the products at different X_{Ti} gave rise to a continuous mass loss from room temperature to *ca.* 400 °C (the TG curves are not shown here). The values of mass loss from room temperature to 400 °C are listed for the products at various X_{Ti} in Table 1. The large mass loss from 24 to 20 mass % is ascribed to the release of OH^-, H_2O, NH_4^+ and NO_3^- because the materials calcined above 400 °C show XRD patterns containing oxides of Fe(III) and Ti(IV) and no IR bands of these ions and H_2O. However, as aforementioned, the N content and intensity of the IR bands, due to H_2O, increase upon addition of Ti(IV), nevertheless the mass loss decreases. This conflict can be solved by considering that replacing Fe(III) with Ti(IV) accompanies the charge compensation by turning OH^- into O^{2-}, leading to a decrease of OH^- content and mass loss by adding Ti(IV). Unfortunately, this is not confirmed by IR because the 3400 cm^{-1} band includes the absorption by HN_4^+ and H_2O.

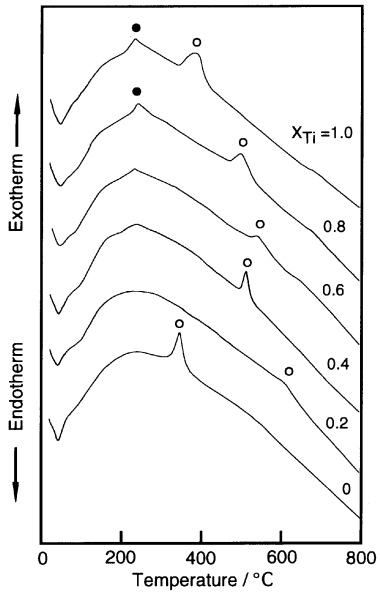

Fig. 4 DTA curves of the products at various X_{Ti}. ●, Crystallization into rutile; ○, crystallization into oxides.

Fig. 4 shows the DTA curves of the products at various X_{Ti}. The DTA curve of the product at $X_{Ti} = 0$ shows an exothermic peak at 375 °C due to crystallization to α-Fe_2O_3 as verified by XRD. The product at $X_{Ti} \geqslant 0.8$ clearly shows an additional exothermic peak at 224 °C, marked by solid circles, due to the crystallization to rutile as confirmed by XRD. The XRD patterns (Fig. 2) showed an additional weak peak at $2\theta = 45°$. These results seem to suggest formation of a new crystal phase in the products at high X_{Ti}. An appreciable bending of the baseline is seen in all the curves, the bending is caused by the heat capacity change accompanied by the phase transformation. The exothermic peak due to the crystallization, marked by open circles, shifts with a change of X_{Ti} while the exothermic peak at 224 °C, due to the transformation into ruitle, does not move. When heated at 600 °C in air for 2 h the products showed XRD peaks of α-Fe_2O_3 (JCPDS 13–534) at $X_{Ti} = 0$ and 0.2, $Fe_2O_3{\cdot}TiO_2$ (9–182) at $X_{Ti} = 0.4$, $Fe_2O_3{\cdot}TiO_2$ and $Fe_2Ti_3O_9$ (29–1494) at $X_{Ti} = 0.6$, $Fe_2Ti_3O_9$ at $X_{Ti} = 0.8$, and TiO_2 [rutile (21–1276) + anatase (21–1272)] at $X_{Ti} = 1.0$; although the XRD patterns are not shown here. Besides these oxide peaks, an unknown peak appears at $2\theta = 55°$ on the products at $X_{Ti} = 0.2$, 0.6 and 0.8. The crystal phase of the oxides formed by heating is thus dependent on the X_{Ti}, which causes a shift in the exothermic peaks of crystallization into oxides.

Mössbauer spectroscopy

The XRD results demonstrate that the products are ferrihydrite particles consisting of crystallites of about 1 nm size. To increase our insight into the structure of the particles, Mössbauer spectroscopy of the products was carried out. This technique is sensitive to the local structures of various iron compounds, so it is an indispensable means for investigation of the nanostructure of iron oxides. Fig. 5 depicts the spectra of the product at $X_{Ti} = 0$, 0.4 and 0.8, recorded at different temperatures from 10 to 300 K. The Mössbauer parameters obtained from the spectra of all the products are listed in Table 2. The spectra taken at 77 and 300 K for the products at $X_{Ti} = 0$ in Fig. 5 show doublet bands that are characteristic of

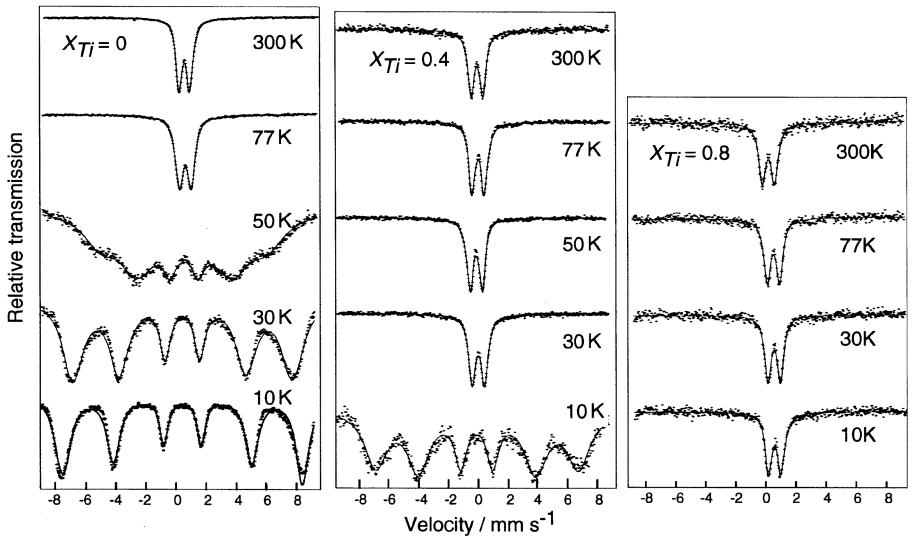

Fig. 5 Mössbauer spectra of the products at $X_{Ti} = 0$, 0.4 and 0.8 recorded at 10–300 K.

the superparamagnetism observed for fine iron oxide particles with a size less of than *ca.* 10 nm.[19,20] This result is reasonable, because the products are nanosized particles (Table 1). As seen in Table 2, the isomer shifts for all the products are essentially the same, meaning that the valency and coordination number is not varied by changing X_{Ti}. The FWHM of the products at $X_{Ti} = 0$ and 0.2 show maximum values of 2.72 mm s^{-1} at 50 K and 2.43 mm s^{-1} at 30 K, respectively, owing to an overlapping of sextet and doublet bands. The hyperfine field (HF) and quadrupole splitting (QS) of the product at $X_{Ti} = 0$ are 48.9 T and -0.01 mm s^{-1} at 10 K, respectively, which are close to the literature values for ferrihydrite at 4 K (HF = 46.5–50.0 T and QS = -0.02–-0.1 mm s^{-1}).[21] This also supports the premise that the products are 2-line ferrihydrite. As seen in Fig. 5, the spectra taken below 30 K for the product at $X_{Ti} = 0$ show the sextet peaks and the spectrum at 50 K is transitional; the superparamagnetism disappears below 30 K. Therefore, the blocking temperature where the superparamagentism is prevented is close to 50 K. The spectrum for the product at $X_{Ti} = 0.4$ possesses sextet bands only at 10 K and for the product at $X_{Ti} = 0.8$ there is only the doublet even at 10 K. The spectrum of the product at $X_{Ti} = 0.6$, not shown in Fig. 5, was also a doublet at 10 K. These results reveal that the blocking temperature of the products is lowered by increasing X_{Ti}. Since the mean particle sizes of 3.3–4.1 nm in Table 1 are not appreciably different, the drop in the blocking temperature by the addition of Ti(IV) is ascribed to a magnetic interaction between the Fe and Ti atoms or to a contraction of the magnetic domains in the particles. Fig. 6 shows the QS values of the doublet bands of the spectra traced below 77 K. The QS decreases with increasing X_{Ti}. This finding can be explained by considering that the disturbance in the local structure around the Fe atoms by the addition of the Ti(IV) decreases the electric field gradient induced by the surrounding ions at the Fe atoms. Kauffman and Hazel[22] have interpreted the band broadening of the Mössbauer spectra by a distribution of the position and nature of ligands such as O, OH and H_2O. Thus, the FWHM is associated with the distortion of the crystal lattice. Fig. 7 plots the FWHM of the sextet and doublet bands of the spectra traced at 10 and 300 K against X_{Ti}. Both the band widths increase with increasing X_{Ti}, indicating that the lattice orientation around the Fe atoms become irregular by adding Ti(IV).

Table 2 Mössbauer parameters for the products

X_{Ti}/ atom %	Temperature/ K	FWHM/ mm s^{-1}	Isomer shift/mm s^{-1}	QS/ mm s^{-1}	HF/T
0	300	0.49	0.33	0.70	
	77	0.63	0.46	0.78	
	50	2.72	0.44	0.05	34.1
	30	1.51	0.47	0.01	44.6
	10	1.01	0.48	−0.01	48.9
0.2	300	0.49	0.33	0.75	
	77	0.50	0.46	0.79	
	50	0.56	0.47	0.80	
	30	2.43	0.52	0.07	36.3
	10	1.26	0.40	0.01	46.5
0.4	300	0.52	0.35	0.79	
	77	0.51	0.46	0.83	
	50	0.51	0.47	0.83	
	30	0.57	0.47	0.84	
	10	1.82	0.48	0.02	41.9
0.6	300	0.52	0.34	0.79	
	77	0.51	0.46	0.81	
	30	0.52	0.46	0.82	
	10	0.92	0.46	0.91	
0.8	300	0.56	0.35	0.81	
	77	0.55	0.45	0.84	
	30	0.53	0.46	0.85	
	20	0.56	0.48	0.85	
	10	0.55	0.49	0.85	

Conclusions

Fe–Ti mixed oxide particles with 3–4 nm size could be produced by the freezing method. The particles obtained were poorly crystalline 2-line ferrihydrite and consisted of crystallites of about 1 nm size corresponding to aggregates of several octahedral units. The products contained an appreciable amount of OH^- and H_2O and a small quantity of NH_4^+.

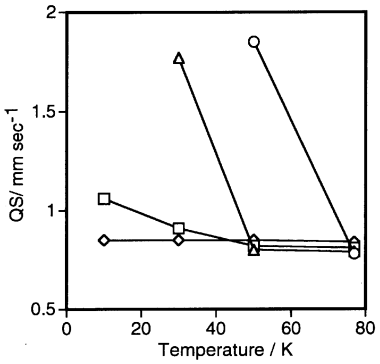

Fig. 6 QS values of the doublet bands of the Mössbauer spectra taken below 77 K for the products at $X_{Ti} = 0$ (○), 0.2 (△), 0.6 (□) and 0.8 (◇).

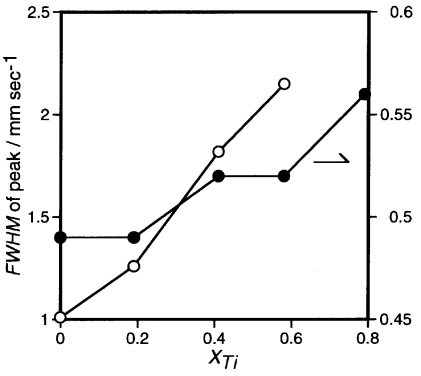

Fig. 7 FWHM of the doublet and sextet bands of the Mössbauer spectra *vs.* X_{Ti}. ●, Doublet band at 300 K; ○, sextet band at 10 K.

When heated above 400 °C all the products turned into the mixed oxides of which the crystal phases depend on X_{Ti}. The products exhibited superparamagnetism at room temperature and the blocking temperature was lowered by the addition of Ti(IV). The local structure of the mixed oxides was disturbed with increasing the Ti(IV) content due to a replacing of the Fe(III) with Ti(IV) in the oxide network, as confirmed by Mössbauer spectroscopy.

Acknowledgement

The authors are grateful to Mr. Masao Fukusumi of Osaka Municipal Technical Research Institute for help with the TEM observations. We also acknowledge Dr. Watanabe, Mr. M. Inaba, and Dr. T. Ohki of Kobelco Research Institute for measuring XAFS and Mössbauer spectroscopy. This study was partly supported by the Grant-in-Aid for Science Research Funds (B) and (C) from the Ministry of Education, Science, Sports and Culture, Japanese Government.

References

1 R. W. Siegel, *Sci. Am.*, 1996(December), 74.
2 S.-L. Chen, P. Dong, G.-H. Yang and J.-J. Yang, *Ind. Eng. Chem. Res.*, 1996, **35**, 4487.
3 H. Weller, *Adv. Mater.*, 1993, **5**, 88.
4 H. Gleiter, *Adv. Mater.*, 1992, **4**, 474.
5 A. A. van der Giessen, *J. Inorg. Nucl. Chem.*, 1966, **28**, 2155.
6 A. A. van der Giessen, *Chemical and Physical Properties of Iron(III)-Oxide Hydrate*, Thesis, Technical University, Eindhoven, May 1968.
7 T. Ishikawa, H. Yamashita, A. Yasukawa, K. Kandori, T. Nakayama and F. Yuse, *J. Mater. Chem.*, 2000, **10**, 543.
8 T. Ishikawa, R. Katoh, A. Yasukawa, K. Kandori, T. Nakayama and F. Yuse, *Corros. Sci.*, 2001, **43**, 1727.
9 T. Ishikawa, M. Kumagai, A. Yasukawa, K. Kandori, T. Nakayama and F. Yuse, *Corros. Sci.*, 2002, **44**, 1073.
10 W. Feitknecht, R. Giovanoli, W. Michaelis and M. Muller, *Helv. Chim. Acta*, 1973, **56**, 2847.
11 F. W. Chukhrov, B. B. Zvyagin, G. Gorshkov, L. P. Yermilova and V. V. Balashova, *Int. Geol. Rev.*, 1973, **16**, 1131.
12 U. Schwertmann and W. R. Fischer, *Geoderma*, 1973, **10**, 237.
13 R. M. Cornell and U. Schwertmann, *The Iron Oxides, Structure, Properties, Reactions, Occurrence and Uses*, VCH, Weinheim, 1996, p. 22.
14 A. Manceau and V. A. Drits, *Clay Miner.*, 1993, **28**, 165.
15 V. A. Drifts, B. A. Sakharov, A. L. Salyn and A. Manceau, *Clay Miner.*, 1993, **28**, 165.
16 K. M. Towe and W. F. Bradley, *J. Colloid Interface Sci.*, 1967, **24**, 384.
17 K. Nakamoto, *Infrared and Raman Spectra of Inorganic and Coordination Compounds*, Wiley, New York, 1986.
18 J. D. Russell, *Clay Miner.*, 1979, **14**, 109.
19 L. Néel, *C. R. Hebd. Seances Acad. Sci.*, 1949, **228**, 664.
20 L. Néel, *J. Phys. Soc. Jpn.*, 1962, **17**(Suppl. B-1), 676.
21 E. Murad and J. H. Johnston, *Iron Oxide and Oxyhydroxides, Mössbauer Spectroscopy Applied to Inorganic Chemisrty*, Plenum, New York, 1987, p. 507.
22 K. Kauffman and F. Hazel, *J. Inorg. Nucl. Chem.*, 1975, **37**, 2155.